

# PROBING THE TRUNCATION OF GALAXY DARK MATTER HALOS IN HIGH DENSITY ENVIRONMENTS FROM HYDRODYNAMICAL N-BODY SIMULATIONS

MARCEAU LIMOUSIN<sup>1</sup>, JESPER SOMMER-LARSEN<sup>1</sup>, PRIYAMVADA NATARAJAN<sup>2,3</sup> & BO MILVANG-JENSEN<sup>1</sup>

*Draft version March 3, 2009*

## ABSTRACT

We analyze high resolution, N-body hydrodynamical simulations of fiducial galaxy clusters to probe tidal stripping of the dark matter subhalos. These simulations include a prescription for star formation allowing us to track the fate of the stellar component as well. We investigate the effect of tidal stripping on cluster galaxies hosted in these dark matter subhalos as a function of projected cluster-centric radius. To quantify the extent of the dark matter halos of cluster galaxies, we introduce the half mass radius  $r_{1/2}$  as a diagnostic, and study its evolution with projected cluster-centric distance  $R$  as a function of redshift. We find a well defined trend for  $(r_{1/2}, R)$ : the closer the galaxies are to the center of the cluster, the smaller the half mass radius. Interestingly, this trend is inferred in *all* redshift frames examined in this work ranging from  $z=0$  to  $z=0.7$ . At  $z=0$ , galaxy halos in the central regions of clusters are found to be highly truncated, with the most compact half mass radius of 10 kpc. We also find that  $r_{1/2}$  depends on luminosity and we present scaling relations of  $r_{1/2}$  with galaxy luminosity. The corresponding total mass of the cluster galaxies is also found to increase with projected cluster-centric distance and luminosity, but with more scatter than the  $(r_{1/2}, R)$  trend. Comparing the distribution of stellar mass to total mass for cluster galaxies, we find that the dark matter component is preferentially stripped, whereas the stellar component is much less affected by tidal forces. We compare these results with galaxy-galaxy lensing probes of  $r_{1/2}$  and find qualitative agreement. Future surveys with space based telescopes such as DUNE and SNAP, that combine wide field and high resolution imaging, will be able to probe the predicted  $(r_{1/2}, R)$  relation observationally.

*Subject headings:* galaxies: dark matter halos – numerical simulations: N-body, hydrodynamical

## 1. INTRODUCTION

The dependence of galaxy properties on environment is well established (see, *e.g.* Adami et al. 1998; Lanzoni et al. 2005; Boselli & Gavazzi 2006; De Lucia 2006). One of the most extreme environments for galaxies is inside a massive galaxy cluster, where active, strong tidal forces are exerted by the global cluster potential. The theoretical expectation is that the global tidal field of a massive, dense cluster potential is strong enough to truncate the dark matter halos of galaxies that traverse the cluster core. Early work (*e.g.* Merritt 1983; Malumuth & Richstone 1984; Merritt 1984) found that a large fraction of the mass initially attached to galaxies in the central Mpc is stripped. Avila-Reese et al. (1999); Bullock et al. (2001); Avila-Reese et al. (2005) found that halos in dense environments are more truncated and more compact than their isolated counterparts of the same luminosity. On galaxy scales, using dark matter only simulations, Diemand et al. (2007) have studied the evolution of subhalos in the Via Lactea host halo, and find that tidal forces remove subhalo mass from the outside in, which leads to higher concentrations for subhalos located in the inner regions compared to field halos of the same mass. Detailed studies of the evolution of subhalos in clusters in dark matter only simulations have been performed by Ghigna et al. (1998, here-

after G98) and De Lucia et al. (2004). G98 find that the dominant interactions in cluster environments are between the global cluster tidal field and individual galaxies after  $z=2$ , and that the cluster tidal field significantly strips galaxy halos. Moreover, both numerical simulations (G98) and analytical calculations (Mamon 2000) predict that the tidal radius of a given galaxy depends on its cluster-centric distance. As a consequence, the closer to the center the galaxies are, the stronger are the tidal forces they will experience, resulting in more compact subhalos. G98 probed the characteristic extent of galaxy subhalos with cluster-centric distance, at  $z=0$  and  $z=0.5$ . Considering the three dimensional cluster-centric distance, they find that subhalo extents decreases towards the cluster center, but this trend was weak and therefore hard to detect at  $z=0.5$ . They argue that this is due to the fact that at  $z=0.5$ , the cluster has quite an anisotropic mass distribution and tides are efficient only at its very center. When considering the *projected* cluster-centric distance, this trend does not totally disappear but becomes marginal, suggesting that subhalo extents do not strongly depend on present day projected cluster-centric distances.

From an observational point of view, gravitational lensing seems the only currently viable method to probe the extent of dark matter subhalos in clusters, and this statement is specially true for cluster galaxies. In the case of field galaxies, satellite dynamics can be used as well (*e.g.* Prada et al. 2003) and gives results consistent with current galaxy-galaxy lensing studies. The deflection caused by galaxy scale mass concentrations is small (quantified by a shear  $\gamma \sim 0.01$ ) and thus is challenging to detect. However,

<sup>1</sup> Dark Cosmology Centre, Niels Bohr Institute, University of Copenhagen, Juliane Maries Vej 30, 2100 Copenhagen, Denmark; marceau@dark-cosmology.dk

<sup>2</sup> Astronomy Department, Yale University, P.O. Box 208101, New Haven, CT 06520-8101, USA

<sup>3</sup> Department of Physics, Yale University, P.O. Box 208101, New Haven, CT 06520-8101, USA

galaxy-galaxy lensing studies in clusters have been performed (Natarajan et al. 1998; Geiger & Schneider 1999; Natarajan et al. 2002a,b; Limousin et al. 2007a) where this shear signal is boosted by the smoothly distributed large scale dark matter distribution. These studies have successfully statistically detected the weak lensing signal generated by cluster galaxies (see also recent work by Halkola et al. 2007). These analyses have provided evidence for truncation of galaxy dark matter halos in high density environments. The inferred typical half mass radius was found to be typically more compact than 50 kpc, whereas half mass radii larger than 200 kpc are derived for field galaxies of equivalent luminosity (Fischer et al. 2000; McKay et al. 2001; Hoekstra et al. 2003, 2004). Moreover, when using the NFW (Navarro et al. 1997) profile, concentration parameters greater than 20 were inferred (Limousin et al. 2006) for some clusters. These results are in qualitative agreement with the tidal stripping scenario. Recently, using a large HST mosaic covering up to 5 Mpc from the center of galaxy cluster Cl0024 at  $z=0.39$ , Natarajan et al. (2008) were able to probe the galaxy population in three radial bins and inferred a larger extent for the halos of galaxies living in the outskirts of the cluster (i.e. at a cluster-centric distance between 3 and 5 Mpc) compared to the galaxies living in the core of the cluster (here between 0 and 3 Mpc).

In this paper, we want to investigate how tidal forces shape the fate of galaxy dark matter halos, and in particular, we focus on the *extent* of cluster galaxy dark matter halos and probe its evolution with cluster-centric distance and redshift. We analyze N-body hydrodynamical simulations of two fiducial galaxy clusters that contain not only dark matter particles but also stars and gas particles that interact through many physical processes. In order to make predictions for future surveys that will constrain the extent of the halos as a function of cluster-centric distance, we consider the *projected* cluster-centric distances since this is what can be probed observationally. The extent of subhalos is quantified by the half mass radius  $r_{1/2}$  since it is directly comparable to the characteristic extent probed via galaxy-galaxy lensing studies.

This paper is organized as follows: in Section 2, we discuss the properties of the two simulated clusters studied here. In Section 3, we investigate how the half mass radius  $r_{1/2}$  and the total mass  $M_{\text{tot}}$  evolve with cluster-centric distance, for different assembly stages (redshift frames) in these simulations. In Section 4, we investigate how  $r_{1/2}$  and  $M_{\text{tot}}$  evolve with luminosity. We fit scaling relations for  $r_{1/2}$ ,  $M_{\text{tot}}$  and the luminosity, and present total mass to light ratios. In Section 5, we investigate the ratio of the total to the stellar mass and its evolution with cluster-centric distance and redshift. In Section 6, we compare galaxy-galaxy lensing results to our theoretical predictions, and finally we present our conclusions in Section 7. All our results in this paper are scaled to the flat, low matter density  $\Lambda$ CDM cosmology with  $\Omega_M = 0.3$ ,  $\Omega_\Lambda = 0.7$  and a Hubble constant  $H_0 = 70 \text{ km s}^{-1} \text{ Mpc}^{-1}$ .

## 2. SIMULATIONS OF OUR FIDUCIAL CLUSTERS

### 2.1. Cluster Properties

N-body hydrodynamical (TREESPH) simulations of the formation and evolution of two galaxy clusters in a  $\Lambda$ CDM

cosmology have been performed. The simulations include metallicity-dependent radiative cooling, star formation according to different initial mass functions, energy feedback as strong starburst-driven galactic superwinds, chemical evolution with non-instantaneous recycling of gas and heavy elements, effects of a metagalactic ultraviolet field and thermal conduction in the intracluster medium. For full details on these simulations and for a comparison of the properties of the simulated clusters to observations, we refer the reader to a series of three papers: Romeo et al. (2006, 2005); Sommer-Larsen et al. (2005), hereafter RSL.

The main difference between the two simulated clusters is their temperature (or equivalently their mass) and the numerical resolution. The more massive cluster is a 6 keV cluster, that we will hereafter refer to as COMA. At  $z=0$ , its virial radius is equal to 2.9 Mpc, and the corresponding virial mass is equal to  $1.3 \times 10^{15} M_\odot$ . The second cluster is a 3.1 keV cluster that we will refer to as VIRGO. At  $z=0$ , its virial radius is equal to 1.8 Mpc, and the corresponding virial mass is equal to  $2.8 \times 10^{14} M_\odot$ . The particle mass in VIRGO is 8 times lower than the one used to simulate COMA. Thus the VIRGO simulation is a higher resolution one and we are able to resolve smaller galaxies. On the other hand, since COMA is a more massive cluster, more massive galaxies than in VIRGO will form.

The highest redshift frame we analyze is  $z=0.7$ . At this redshift, both clusters are virialized and there is a clear dominant cluster halo. At higher redshifts, the clusters are not well defined (no clear dominant halo) and are still under construction with major merger events. However, for any redshift slice, COMA is less relaxed than VIRGO. In the case of COMA at  $z=0.7$ , simulations reveal some infalling galaxies, whereas that is not the case in VIRGO. This difference in dynamical states can be quantified by the redshift of the last major merger event: for COMA, the last merger event occurs at around  $z=0.8$ , whereas it is at around  $z=1.5$  for VIRGO. This means that COMA is dynamically younger than VIRGO, and, as we will see, the VIRGO galaxy population is more relaxed, with less scatter in the relations we study in this work. Due to the difference in dynamical states between the two simulated clusters, it is not easy to directly compare their respective properties, in the sense that COMA is not simply a rescaling of VIRGO at a higher temperature. Pictures and movies of the simulated clusters can be found at <http://www.tac.dk/~jslarsen/Clusters/>

### 2.2. Extracting subhalos from the simulated clusters

The first step of our analysis is to extract substructures from the simulated cluster in order to get a catalog of cluster galaxies. This procedure is detailed in RSL and summarized below. In order to ascertain that we identify all galaxies, and hence sub-halos, in the main cluster halo the following approach was adopted. A cubic grid of cube-length  $\Delta l=10$  kpc is overlaid the cluster, and all cubes containing at least  $N_{\text{th}}=2$  star particles are identified. Subsequently, each selected cube is embedded in a larger cube of cube-length  $3\Delta l$ . If this larger cube contains at least  $N_{\text{min}}=7$  star particles, which are gravitationally bound by its content of gas, stars and dark matter the system is identified as a potential galaxy. Since the method can return several, almost identical versions

of the same galaxy only the one containing the largest number of star particles is kept and classified as a galaxy. We tested the galaxy identification algorithm by varying  $\Delta l$ ,  $N_{\text{th}}$ ,  $N_{\text{min}}$ , and also the numerical resolution, and found it to be adequately robust for the purposes of this paper.

### 2.3. Subhalos Properties

Once the subhalos have been identified, galaxy half mass radii,  $r_{1/2}$ , and total masses,  $M_{\text{tot}}$ , were determined by an iterative approach, described below. For a given galaxy the density of the smooth cluster "background" of dark matter and hot, intra-cluster gas at the position of the galaxy is determined. This is done by calculating the average total density in 5 kpc thick shells of radii from  $r_s$  to  $1.5 r_s$ . The "search radius",  $r_s$ , is initially set to  $4 r_t$ , where  $r_t$  is the tidal radius of the galaxy at its position in the cluster defined by (Binney & Tremaine 1988):

$$r_t = r_p \left( \frac{m}{3M} \right)^{1/3} \quad (1)$$

All shells containing other substructures, i.e., galaxies and/or dark matter halos, are subsequently removed using a background density fluctuation criterion, and finally the background density is determined from the remaining shells. Second, the cumulative mass of the galaxy, including its dark matter halo (above the background density) is determined in 2.5 kpc thick shells, going from inside and out, until a shell is reached of density equal to or less than that of the background. Using the cumulative mass distribution, the half mass radius  $r_{1/2}$ , is subsequently determined by linear interpolation. Third, the search radius is set to  $4 r_{1/2}$ , and the above procedure is redone. This is done repeatedly until convergence. Tests with different parameter values show the above procedure to be an efficient and robust way for determining half mass radii and total masses of cluster galaxies.

By construction,  $r_{1/2}$  is the radius within which the 3D mass of the simulated galaxies equals half of the total mass. We will refer to this quantity as being the 3D half mass radius. We also pursue a 2D analysis. In particular, we looked at  $R_{1/2}$ , the radius within which the 2D mass equals half of the total mass, as described below. Once we know the 3D region (assumed spherical) where a given galaxy is confined and contained, we projected the excess mass density in this region (above the cluster mean density) onto the plane along the three cardinal directions, and averaged over the results. This gives us a robust estimate of the 2D projected mass, that we use to calculate  $R_{1/2}$ . We will refer to this quantity as the 2D half mass radius. We will compare these quantities in Section 3. However, when looking at possible scalings of the half mass radius with luminosity, we will use  $r_{1/2}$  only. The quantity  $r_{1/2}$  is robust as it is easily calculated and well defined for most popularly used mass models. Moreover,  $r_{1/2}$  is not the result of an average of projected quantities, thus in principle a less noisy quantity than  $R_{1/2}$ .

There is a large scatter in the properties of the galaxies that form in these cluster simulations. This scatter is mainly due to the diverse orbital histories of galaxies. To consolidate results, we define bins, in which we compute

the median of the points as well as the standard deviation  $\sigma$ . The error is defined as  $\sigma/\sqrt{N}$ , where  $N$  is the number of objects in a given bin. In the following, when needed, we fit a linear function to the points corresponding to the galaxies, and not to the binned data.

### 2.4. Projected cluster-centric distance

Since observational probes are sensitive to *projected* cluster-centric distances, we project the 3D radial distance of the galaxies with respect to the center of the cluster over the three cardinal axes, and our cluster galaxy catalog is made by merging the three catalogs corresponding to each projection. We thus artificially increase the data by a factor of three. This is not unreasonable to do since we can imagine that three different observers have been looking at the cluster from the three cardinal axes and have merged their corresponding data sets. This procedure is equivalent to observing three different clusters in a similar dynamical state. It is important at this point to make sure that the relation between half mass radius and projected cluster-centric distance we aim to probe does not depend on the adopted viewing angle and that we do not introduce any systematics by merging catalogs corresponding to each projection. To this purpose, we have looked at the evolution of the half mass radius with respect to the three different projections of the cluster-centric distance. We find no bias. To illustrate this point, we show on Fig. 1 the evolution of the half mass radius as a function of the projected cluster-centric distances, considering the binned data and the VIRGO cluster. We see that the relation does not depend on the adopted projected cluster-centric distance. The same conclusion can be drawn when considering the unbinned data points. Moreover, we reach similar conclusions in the case of the COMA cluster. Also shown for comparison is the relation when merging the data sets as done in the rest of the paper. Note that looking at possible variations with viewing angle is interesting from an observational perspective and suggests that projection effects are not important for observational studies.

## 3. TRENDS WITH CLUSTER-CENTRIC DISTANCE

The extent and efficiency of tidal stripping depends primarily on the details of the orbital parameters of the subhalo. In this Section, we study the evolution of the half mass radii ( $r_{1/2}$ ,  $R_{1/2}$ ) and the total mass  $M_{\text{tot}}$  as a function of the projected cluster-centric distance  $R$ , for different redshift frames. In Fig. 2, we plot  $r_{1/2}$  and  $R_{1/2}$  as a function of  $R$  both for VIRGO and COMA, for the two redshift frames we consider, i.e.  $z=0$  and  $z=0.7$ . We clearly see that both the  $(r_{1/2}, R)$  and  $(R_{1/2}, R)$  trends are well defined, at *any* redshift. Closer to the center of the cluster the extent of the dark matter halos of the cluster galaxies is smaller. Thus closer to the center of the cluster, stronger tidal stripping is experienced by galaxies. The  $(r_{1/2}, R)$  and  $(R_{1/2}, R)$  trends are illustrated on Fig. 2 for the two extreme redshift frames considered in the simulations,  $z=0$  and  $z=0.7$ . This choice is motivated by clarity of the figure and to enhance the evolution between  $z=0$  and  $z=0.7$ . These trends are inferred in all redshifts frames extracted from the simulations ( $z=0$ ,  $z=0.2$ ,  $z=0.4$  and  $z=0.7$ ). Note that if this trend is inferred both at  $z=0$  and  $z=0.7$ , then it must be present for intermediate redshifts as well.

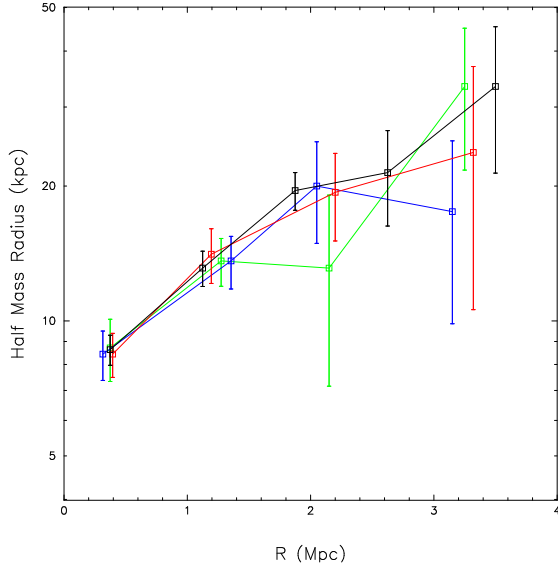


FIG. 1.— median half-mass radii  $r_{1/2}$  as a function of projected cluster-centric distance in VIRGO. This cluster-centric distance corresponds to the projection of the 3D cluster-centric distance along the three cardinal axes: along the  $x$  axis (green), the  $y$  axis (red) and the  $z$  axis (blue). Also show is the relation when merging the three data sets (black) which corresponds to the solid line in the upper left panel of Fig. 2. We see no bias with viewing angle.

We see that for any given  $R$ ,  $r_{1/2}$  and  $R_{1/2}$  are systematically smaller at lower redshift compared to the high redshift frame: by  $z=0$ , the galaxies have had more passages through the cluster center, have been stripped more and thus have a smaller extent. As expected, we see that the 2D half mass radius  $R_{1/2}$  is systematically smaller than the 3D half mass radius  $r_{1/2}$ .

In Fig. 2, we plot the total mass  $M_{\text{tot}}$  as a function of  $R$  both for VIRGO and COMA, for the two redshift frames we consider. At  $z=0$ , we infer a  $(M_{\text{tot}}, R)$  trend, but the scatter is larger than the one associated with the  $(r_{1/2}, R)$  trend. This difference in trends can be understood as follows: consider a galaxy of mass  $m$  with a circular velocity  $v_c$  located in the cluster whose mass is  $M$ , we can relate the scatter on the tidal radius ( $\delta r_t/r_t$ ) to the scatter on the galaxy mass ( $\delta m/m$ ). The tidal radius of the galaxy is proportional to:

$$r_t \propto \left(\frac{m}{3M}\right)^{1/3} \quad (2)$$

(Eq. 1) and the mass of the galaxy is given by:

$$m \propto r_t v_c^2, \quad (3)$$

thus  $r_t \propto r_t^{1/3} v_c^{2/3}$ , so  $r_t \propto v_c$  and  $\delta r_t \propto \delta v_c$ . Differentiating Eq. 3, we can write:

$$\delta m = \delta r_t v_c^2 + r_t 2 v_c \delta v_c \propto 3 \delta v_c v_c^2 \quad (4)$$

Combining Eq. 3 and 4, we get:

$$\frac{\delta m}{m} = \frac{3 \delta v_c v_c^2}{r_t v_c^2} = 3 \frac{\delta r_t}{r_t} \quad (5)$$

Therefore finding a larger relative scatter in the  $(M_{\text{tot}}, R)$  trend than in the  $(r_{1/2}, R)$  trend is to be expected. Note that at  $z=0.7$ , COMA is not well relaxed and some galaxies have not experienced the tidal field of the cluster potential yet. As a consequence, the outer radial bin contains some infalling galaxies which have values of

$r_{1/2}$  and total masses typical of field galaxy values (i.e.  $r_{1/2} > 200$  kpc and  $M_{\text{tot}} > 10^{12} M_\odot$  as obtained from galaxy-galaxy lensing and satellite dynamics analysis, see Section 1).

In Fig. 2, we also show the results from G98 at  $z=0$ . G98 studied a simulated galaxy cluster with virial radius 1.95 Mpc and virial mass  $2.8 \times 10^{14} M_\odot$ . These properties makes it very similar to our VIRGO cluster. Thus we compare their results (data points with triangle) to ours on VIRGO, for the redshift frame at  $z=0$  (solid line). We find significant differences between our results and the one from G98. Before discussing these differences, we want to caution that both works are different and difficult to compare. Therefore, the disagreement between these studies cannot be used to assess quantitatively the impact of the baryonic component in the tidal stripping process. We also note that there could be significant differences in subhalo finding algorithms. Keeping that in mind, three statements can be made from this comparison: data points from G98 have larger error bars and are systematically higher than ours. Moreover, the clear trend we infer appears marginal in the work by G98. The difference in the error bars comes from the statistics: within 2 Mpc, G98 identified  $\sim 200$  halos whereas we have  $\sim 650$  halos within the same radius. The difference in the value of  $r_{1/2}$  can be partly due to the difference in resolution: G98 use particles whose mass is  $8.6 \times 10^8 M_\odot$  whereas we use particles whose masses are  $4.4 \times 10^7 M_\odot$  and  $3.2 \times 10^8 M_\odot$  for the stellar and dark matter respectively. The mass of our individual particles is 3-20 times smaller, thus we resolve smaller galaxies than G98: they adopt a minimum of 32 particles to define a halo whose individual properties are relevant, which translates into a minimum mass of  $2.7 \times 10^{10} M_\odot$ . In VIRGO we have 477 galaxies of total mass smaller than this threshold. Therefore our sample is more complete in the inclusion of lower galaxy masses compared to the G98 sample. Since smaller galaxies tend to have smaller extents, this could explain the shift between our results.

In order to properly investigate the role of the baryonic component in the tidal stripping process, we would need a devoted dark matter only simulation of VIRGO and COMA. Such simulations are underway, and will be presented and analysed in a forthcoming publication, where we will be able to quantify the differences expected.

#### 4. SCALING OF $r_{1/2}$ AND $M_{\text{tot}}$ WITH LUMINOSITY & TOTAL MASS TO LIGHT RATIO

Parametric strong lensing studies (*e.g.* Kneib et al. 1996; Tyson et al. 1998; Natarajan et al. 1998; Limousin et al. 2007b) do include the galaxies living in the core of the cluster in the modeling since they can locally perturb strong lensing features. In order to reduce the number of free parameters in lens modeling, the standard approach consists of scaling the galaxy parameters with luminosity as follows:

$$r_{1/2} \propto L^\alpha \quad \& \quad M_{\text{tot}} \propto L^\delta \quad (6)$$

Galaxy-galaxy lensing studies also use similar scaling laws. The scaling usually used for the half mass radius in lensing studies is:  $\alpha = 0.5$ , which assumes that the mass to light ratio is constant for all galaxies. At the present time strong lensing studies are not in a position to discriminate between different scaling relations

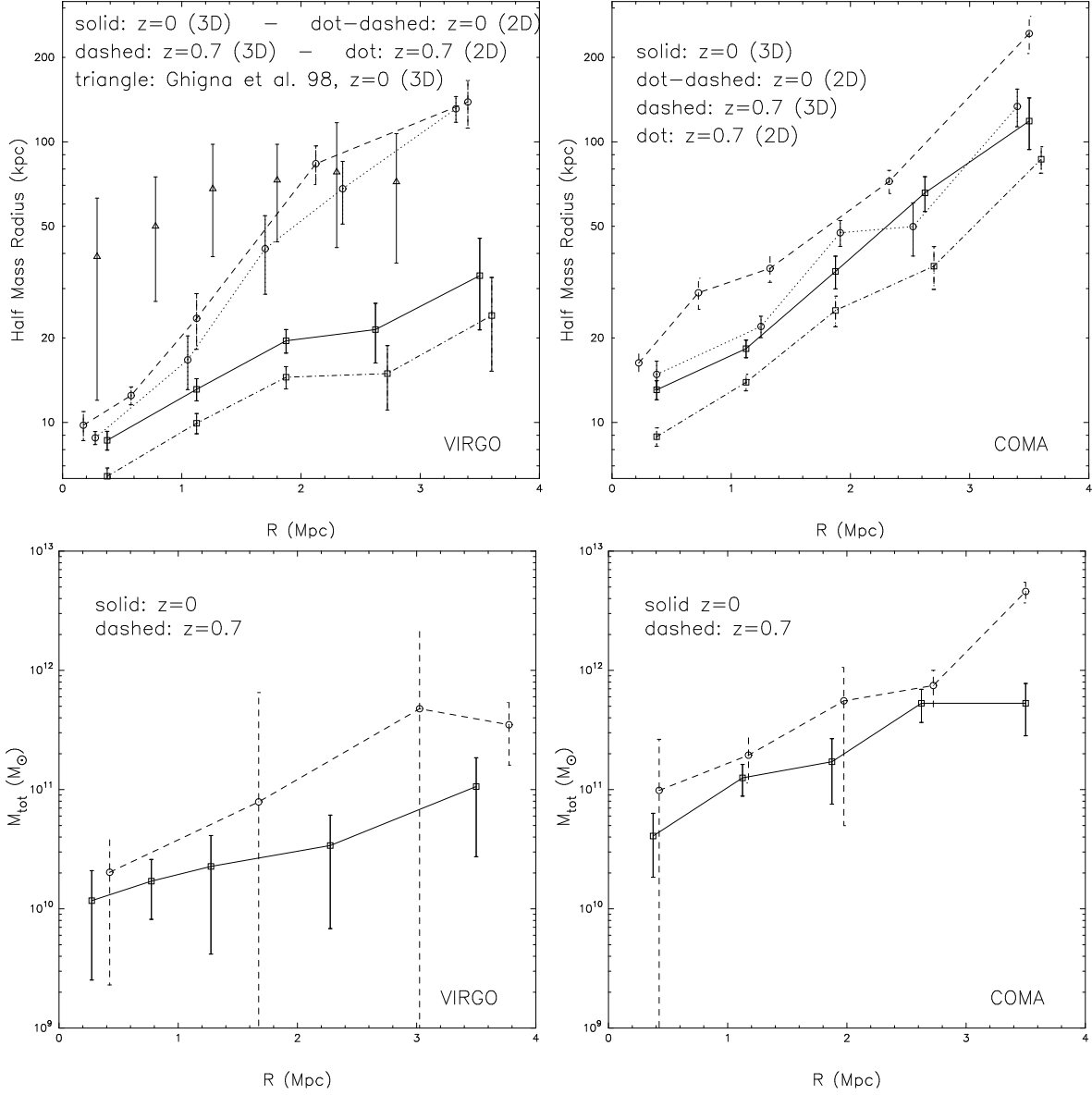


FIG. 2.— Upper panels: median half-mass radius  $r_{1/2}$  (3D) and  $R_{1/2}$  (2D) as a function of projected cluster-centric distance, for  $z=0$  and  $z=0.7$ ; VIRGO (left) and COMA (right). For both clusters, the  $(r_{1/2}, R)$  and  $(R_{1/2}, R)$  trends are clearly defined in *both* redshift slices. Also shown for comparison with VIRGO are the data point from G98 at  $z=0$ . As we could have expected, we see that the 2D half mass radius  $R_{1/2}$  is systematically smaller than the 3D half mass radius  $r_{1/2}$ . Lower panels: median total mass as a function of projected cluster-centric distance, for  $z=0$  and  $z=0.7$ ; VIRGO (left) and COMA (right). For both clusters at  $z=0$ , we find a well defined  $(M_{\text{tot}}, R)$  trend, though the scatter is larger than in the  $(r_{1/2}, R)$  or  $(R_{1/2}, R)$  trends. At high redshift, the scatter is larger and the  $(M_{\text{tot}}, R)$  trend becomes marginal.

(Halkola et al. 2007; Jullo et al. 2007). In order to study the possible value of the exponents defined by Eqn. 6 that could be used in strong lensing modeling, we want to examine the evolution of the half mass radius  $r_{1/2}$  and the total mass  $M_{\text{tot}}$  with luminosity  $L$ , as a function of redshift. We consider the galaxies located in the core of the cluster. (i.e. the galaxies that satisfy  $R < 500$  kpc) since strong lensing modeling deals with the inner part of a galaxy cluster (typically the central  $100''$ ). In Fig. 3 (upper panels), we plot  $r_{1/2}$  as a function of luminosity  $L$  both for VIRGO and COMA, at  $z=0$  and  $z=0.7$ . We fit a linear relation to the unbinned data points for each redshift frame (i.e.  $z = 0, 0.2, 0.4, 0.7$ ) in order to probe the exponent of the scaling relations defined by Eqn. 6. The results are presented in Table 1, and the best linear fit is plotted on Fig. 3. We also fit a linear relation to the unbinned data points corresponding to the  $(M_{\text{tot}}, L)$  trend (Table 1). We find increasing  $(r_{1/2}, L)$  and  $(M_{\text{tot}}, L)$  trends at both redshifts, for the COMA and VIRGO central populations. Looking at the evolution of  $\alpha$  and  $\delta$  with redshift, we do not infer any clear trend of evolution of these values with redshift, thus we average the exponents from the different redshift frames and we consider the averaged values in what follows. Comparing VIRGO and COMA, we see that the scatter is smaller in the case of VIRGO which is more relaxed than COMA (see error bars on the linear fitting results in Table 1).

We caution that we do not claim to have derived fundamental scaling relations here, but rather have fitted to our data sets. As can be seen in Fig. 3, it is clear that the relations likely have a more complicated form than a linear fit.

These inferred scalings can be compared to the fundamental plane derived for early-type galaxies in clusters. The values of  $\delta$  derived in this work are in good agreement with the fundamental plane analysis at  $z=0$  for early-type galaxies ( $\delta = 1.35 \pm 0.15$ ; Jørgensen et al. 1996).

On Fig. 3 we plot the total mass to light ratio  $M_{\text{tot}}/L$  as a function of luminosity. We find that  $M_{\text{tot}}/L$  can reach values as high as 55, with a mean value around  $\sim 20$ -30. It is interesting to compare these total mass to light ratios to stellar mass to light ratios ( $M/L$ ) inferred observationally. Recent studies (Jørgensen et al. 2006, 2007) present a relation between the galaxy masses and the mass to light ratios, for galaxy clusters in the local Universe ( $z=0$ ) and in the high redshift Universe ( $z=0.8 - 0.9$ ). The relations given by Jørgensen et al. (2006) were derived in the B band. We converted their B band luminosities into the R band luminosities using a constant ( $B - R = 2$ ) and inverted the relations in order to get a relation between the stellar mass to light ratio and the R band luminosity:

$$\log\left(\frac{M}{L_R}\right) = \gamma \log(L_R) + \varsigma \quad (7)$$

for  $z=0$ , we find:

$$\gamma = 0.316 \pm 0.03 \quad \& \quad \varsigma = -2.7$$

and for  $z=0.8$ :

$$\gamma = 1.18 \pm 0.08 \quad \& \quad \varsigma = -13.1$$

We plot on Fig. 3 the lines corresponding to the range allowed by these relations. Obviously the total mass to

light ratios  $M_{\text{tot}}/L$  derived in this work are systematically higher than stellar  $M/L$ 's inferred observationally. This can be understood by the fact that we consider the total mass, corresponding to both the baryonic and the dark matter components, whereas the observational  $M/L$  ratio is the stellar mass to light ratio.

We did the same exercise for the whole galaxy population (i.e. for all cluster-centric radii) to compare the  $(r_{1/2}, L)$  and  $(M_{\text{tot}}, L)$  trends inferred for the whole population to the one inferred for the central population ( $R < 500$  kpc). When considering the whole galaxy population, we find increasing  $(r_{1/2}, L)$  and  $(M_{\text{tot}}, L)$  trends at  $z=0$ , both for COMA and VIRGO. On the other hand, at  $z=0.7$ , these trends are hardly defined and the scatter dominates, specially in the case of the  $(M_{\text{tot}}, L)$  trend.

This comparison suggests that in the core of the cluster at high redshift, the galaxy population is already well relaxed and constitutes a homogeneous galaxy population, whereas the galaxies at larger distances from the cluster center have more complicated dynamics. It appears that clusters have a 'well behaved relaxed nucleus' at high redshift. With time this relaxed behavior propagates itself outward into the outskirts of the cluster, resulting at  $z=0$  in a overall 'well behaved' galaxy population.

## 5. DISTRIBUTION OF STARS AND DARK MATTER IN INDIVIDUAL GALAXIES

In order to get insight on how tidal stripping modifies the different galaxy mass components, we study the ratio of the total mass to the stellar mass and its evolution with redshift and cluster-centric distance. First, we verify that there is no dependence of the stellar mass with  $R$ . We find that the scatter in the stellar mass of the galaxy sample is large, and there is no discernable trend with  $R$  at any redshift, suggesting that the stellar component, on average, remains roughly unaffected by tides.

Then, we study the ratio of the total to the stellar mass,  $M_{\text{tot}}/M_*$  and its evolution with both cluster-centric distance and redshift. Fig. 4 shows the result for  $z=0$  and  $z=0.7$ . The ratio of the total to the stellar mass clearly increases with cluster-centric distance. Since tidal forces remove subhalo mass from the outside in (Diemand et al. 2007), this result suggests that the extent of the dark matter subhalo (quantified by  $r_{1/2}$ ) is larger than the extent of the stellar component (quantified by  $r_{1/2}^*$ , the half light radius) even in the very central part of the cluster. To investigate this further, we compare the extent of the stellar component  $r_{1/2}^*$  with  $r_{1/2}$ . We find that  $r_{1/2}^*$  does not depend on the cluster-centric distance  $R$  for any redshift, both for COMA and VIRGO. In addition, for VIRGO, we find that  $r_{1/2}^*$  is compact  $< 2$  kpc, whereas  $r_{1/2} > 8$  kpc (Fig. 2, upper left panel, central bin). For COMA, we find that  $r_{1/2}^* < 3$  kpc, whereas  $r_{1/2} > 11$  kpc (Fig. 2, upper right panel, central bin). This shows that for even the most stripped halos in the central bin,  $r_{1/2}$  is still  $\sim 4$  times larger than  $r_{1/2}^*$ , suggesting that the dissipational stellar component is more compact and not as affected by tides.

## 6. COMPARISON WITH GALAXY-GALAXY LENSING RESULTS

TABLE 1  
DERIVING THE SCALING RELATIONS DEFINED IN EQ. 6

Redshift	0	0.2	0.4	0.7	MEAN
COMA	$\alpha = 0.315 \pm 0.111$ $\delta = 1.431 \pm 0.119$	$\alpha = 0.165 \pm 0.136$ $\delta = 1.297 \pm 0.148$	$\alpha = 0.274 \pm 0.090$ $\delta = 1.189 \pm 0.098$	$\alpha = 0.194 \pm 0.059$ $\delta = 0.983 \pm 0.077$	$\alpha = 0.237 \pm 0.045$ $\delta = 1.22 \pm 0.055$
VIRGO	$\alpha = 0.404 \pm 0.050$ $\delta = 1.303 \pm 0.072$	$\alpha = 0.213 \pm 0.036$ $\delta = 0.905 \pm 0.068$	$\alpha = 0.275 \pm 0.036$ $\delta = 0.963 \pm 0.064$	$\alpha = 0.382 \pm 0.031$ $\delta = 1.186 \pm 0.053$	$\alpha = 0.318 \pm 0.02$ $\delta = 1.09 \pm 0.03$

In this Section, we compare the results from our simulated galaxy population with the results derived from observational galaxy-galaxy lensing studies in clusters. We first need to be sure we compare things that are comparable. The quantity we use from the simulation is the 3D half mass radius  $r_{1/2}$ . Former galaxy-galaxy lensing analyses performed through clusters have used a parametric model to fit the lensing data, the so-called Pseudo Isothermal Elliptical Mass Distribution (PIEMD, see *e.g.* Limousin et al. 2005). This profile is parametrized using two characteristic radii, the core radius and the scale radius (respectively  $r_{\text{core}}$  and  $r_{\text{cut}}$  in former articles). In galaxy-galaxy lensing analyses, since we cannot constrain it, we usually fix the core radius to an arbitrary small value, making this PIEMD profile equivalent to the Brainerd et al. (1996) profile. As a result of the galaxy-galaxy lensing fit, we get some constraints on this scale radius. It is easy to show (Elíasdóttir et al. 2007) that the scale radius for the PIEMD profile without a core radius is equal to the radius within which the 3D mass equals half of the total mass. Thus this parameter inferred from the galaxy-galaxy lensing analysis can be reliably compared to  $r_{1/2}$  from the simulation. It can also be shown (Elíasdóttir et al. 2007) that for a PIEMD profile without a core radius, the radius within which the 2D mass equals half of the total mass is found to be at  $3/4$  of the scale radius.

Of course, lensing is sensitive to the 2D projected surface mass density, and it may be confusing to state that we infer a scale radius related to the 3D properties of the halo from a lensing analysis. However, the 2D projected mass density we are sensitive to with lensing is a function of a scale radius that turns out to be the radius within which the 3D mass equals half of the total mass.

We perform the comparison only with COMA since it is a 6 keV cluster and therefore more similar to the massive, lensing clusters studied observationally than VIRGO. Note that if need be, it is possible to rescale the  $r_{1/2}$  values found for the COMA galaxies to the temperature of a cluster probed observationally using the scaling relation:  $r_{1/2} \propto T^{-1/2}$ . The temperature of a cluster characterized by a velocity dispersion  $\sigma$  scales as:  $T \propto \sigma^2$ , and its mass  $M$  at a cluster-centric distance  $r_c$  scales as:  $M \propto \sigma^2 r_c$ . From Eq. 2 and 3, we can derive that the tidal radius of a galaxy orbiting in the cluster with a circular velocity  $v_c$  scales as:

$$r_t \propto \frac{v_c^{2/3} r_t^{1/3}}{\sigma^{2/3} r_c^{1/3}} r_c \quad (8)$$

so  $r_t \propto v_c r_c / \sigma$ , and finally  $r_t \propto T^{-1/2}$ . This means that the more massive a galaxy cluster is (thus the more dense the environment), the more severe the tidal trun-

cation. For the purpose of the comparison with observed clusters, all apparent magnitudes have been converted to the absolute rest frame R band magnitude. We will apply the same selection criteria (magnitude cut-offs) to the simulated galaxies in order to compare the same luminosity galaxy population to the one probed in galaxy-galaxy lensing studies. Finally, the galaxy-galaxy lensing results have been rescaled to the median value of the luminosity of the simulated galaxy population, using the scaling laws defined in Eq. 6 with  $\alpha = 0.5$  and  $\delta = 1.0$ .

In particular, we compare the results presented in the previous sections with the work by Limousin et al. (2007a), which probes the cluster population down to a magnitude of -17.5 for a sample of five galaxy clusters at redshift around 0.2, with a mean x-ray temperature of 8.5 keV. As discussed in detail in Limousin et al. (2007a), these detections are in agreement with the similar studies performed by Natarajan et al. on observed clusters ranging from  $z = 0.17 - 0.58$  with space based HST data (Natarajan et al. 2007). Fig. 5 shows the comparison. We find qualitative agreement. However, due to the weakness of the galaxy-galaxy lensing signal and the limitations of ground based data, error bars on the estimated parameters are still rather large. Also shown in Fig. 5 is the slope derived for the trend of the variation of typical subhalo mass (mass of a subhalo that hosts an  $L^*$  early-type galaxy) as a function of cluster-centric radius for the massive lensing cluster Cl0024+16 derived from space-based data. The data-set comprises of an HST mosaic that samples out to 5 Mpc from the cluster center and the constraints on the subhalo mass are derived applying galaxy-galaxy lensing methods in 3 radial bins. Strong and weak lensing constraints are combined to derive the average properties of a typical dark matter subhalo that hosts an  $L^*$  early-type galaxy in each radial bin. The variation of the mass of the fiducial subhalo with cluster-centric radius is well-fit by a linear relation. While the slope of this relation can be directly compared to that derived from the simulated COMA cluster (as shown by the dashed line in Fig. 4) the normalization cannot be compared as the central density of Cl0024+16 is significantly higher. We find that the trend derived from these space-based lensing observations is in agreement with the results of the simulations.

## 7. CONCLUSIONS

Using high resolution, hydrodynamical N-body simulations of two fiducial galaxy clusters, one with parameters typical of COMA and the other VIRGO, we study the tidal stripping process in detail. These are the first simulations that include the baryonic component that have been used to study this process, previous studies

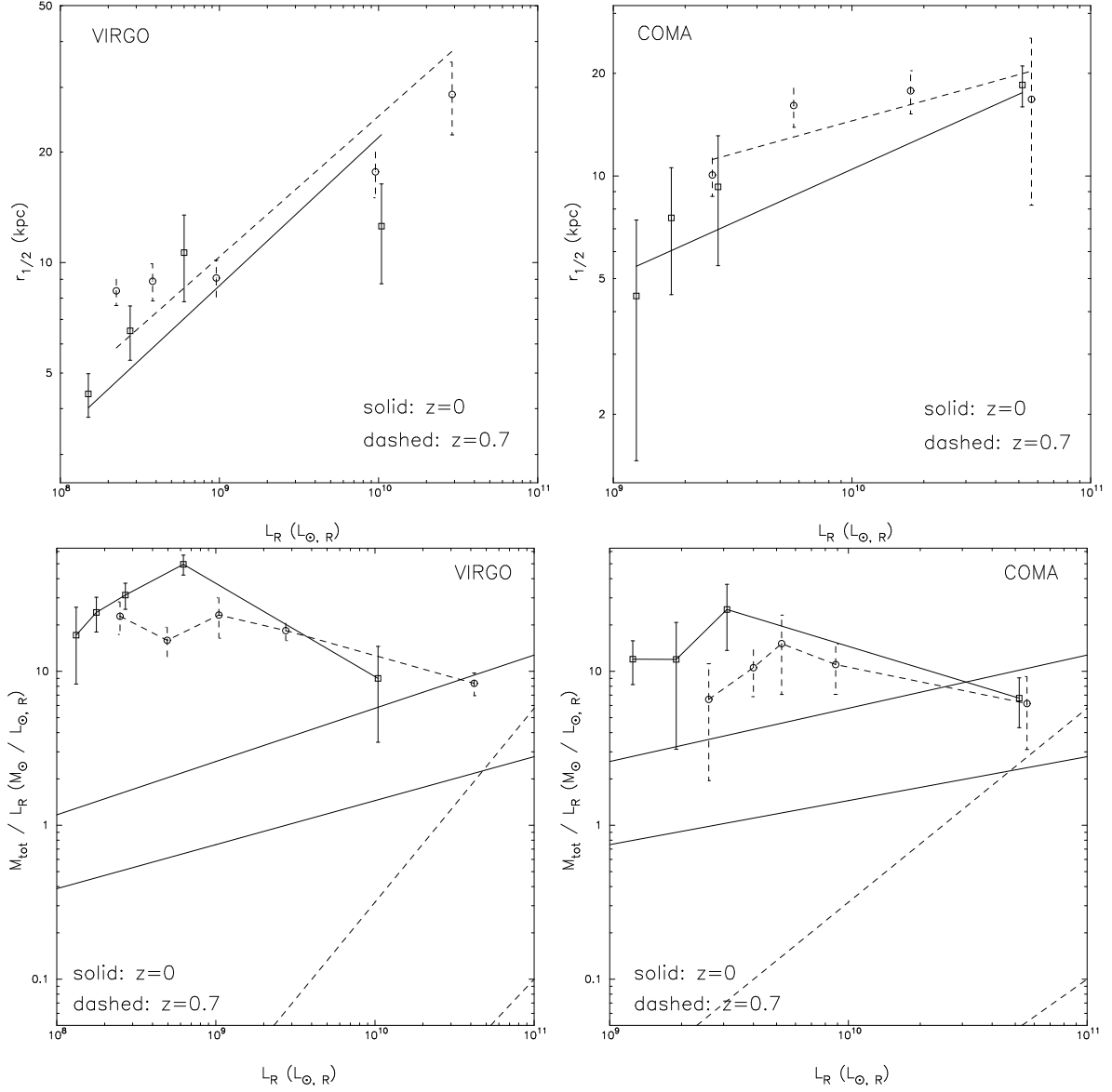


FIG. 3.— Upper panels: median half mass radius  $r_{1/2}$  as a function of luminosity for the central galaxies sample ( $R < 500$  kpc), for  $z=0$  (solid squares) and  $z=0.7$  (dashed circles); VIRGO (left) and COMA (right). Shown is the best fitting linear relation to the unbinned data points (Table 1). We find that  $r_{1/2}$  increases with luminosity, but has a larger scatter in the higher redshift slice. Lower panels: median total mass to light ratio as a function of luminosity for the central galaxies sample for  $z=0$  and  $z=0.7$ ; VIRGO (left) and COMA (right). Overplotted lines correspond to the range allowed by the fundamental plane analysis by Jørgensen et al. (2006). Note different axis scalings in the figure panels.



were limited to dark matter only simulations. We infer a strong trend between the extent of cluster galaxy dark matter subhalos quantified by the half mass radius  $r_{1/2}$  and the projected cluster-centric distance  $R$ . We show that the dark matter component is preferentially stripped, whereas the stellar component is much less affected by tidal forces. We infer a trend in these simulations that is much stronger than the one inferred from the dark matter only cosmological N-body simulations of Ghigna et al. (1998). This could suggest that tidal stripping is more efficient in the inner regions of clusters when the effects of baryons are included. However, we caution that comparing both simulations is not easy and therefore we cannot assess reliably the impact of the baryonic component in the tidal stripping process at this point. What is needed now is a devoted dark matter only simulation of VIRGO and COMA in order to compare reliably the outputs of each study and investigate the expected influence of the baryonic component on the tidal stripping process.

With the next generation of space telescopes, in particular with wide field space based imagers, such as DUNE<sup>4</sup> and SNAP<sup>5</sup>, we will be able to probe this trend in a sample of galaxy clusters spanning different range of masses and dynamical states. The limiting aspect of these kind of studies are the relatively small mass of the dark matter subhalos associated with cluster galaxies (leading to a small modulation in the overall tangential shear field making detection challenging), and therefore the large number of background sources with

reliable shape measurements needed for the lensing analysis. A very promising technique will be the use of future radio and millimeter-wave interferometers: accurate measurements of the detailed dynamical structure of the background galaxies, in particular rotating disks, should make it possible to probe the shear directly on each individual galaxy, thus allowing shear measurements with much less galaxies than it is currently done (Blain 2002; Morales 2006).

From the numerical point of view, what is needed is a sample of galaxy clusters that span a wide range in mass and dynamical states in a large simulation box including baryonic physics, so that a robust comparison between observations and theoretical expectations can then be made. Such a quantitative comparison will be possible in the near future and will provide further insights into the physics of cluster assembly and the process of tidal stripping.

#### ACKNOWLEDGMENTS

The authors gratefully acknowledge the Dark Cosmology Centre at the Niels Bohr Institute, University of Copenhagen. The Dark Cosmology Centre is funded by the Danish National Research Foundation. We thank Roser Pelló for providing us her code that allows to convert magnitudes in different filters to absolute rest frame magnitudes and for help in using it. We thank Árdís Elíasdóttir, Gary Mamon, Jean-Paul Kneib, Jens Hjorth and Mark Wilkinson for useful discussions.

<sup>4</sup> www.dune-mission.net

<sup>5</sup> www.snap.lbl.gov

#### REFERENCES

- Adami, C., Biviano, A., & Mazure, A. 1998, *A&A*, 331, 439
- Avila-Reese, V., Colín, P., Gottlöber, S., Firmani, C., & Maulbetsch, C. 2005, *ApJ*, 634, 51
- Avila-Reese, V., Firmani, C., Klypin, A., & Kravtsov, A. V. 1999, *MNRAS*, 310, 527
- Binney, J. & Tremaine, S. 1988, *S&T*, 76, 45
- Blain, A. W. 2002, *ApJ*, 570, L51
- Boselli, A. & Gavazzi, G. 2006, *PASP*, 118, 517
- Brainerd, T. G., Blandford, R. D., & Smail, I. 1996, *ApJ*, 466, 623
- Bullock, J. S., Kolatt, T. S., Sigad, Y., Somerville, R. S., Kravtsov, A. V., Klypin, A. A., Primack, J. R., & Dekel, A. 2001, *MNRAS*, 321, 559
- De Lucia, G. 2006, *ArXiv Astrophysics e-prints*
- De Lucia, G., Kauffmann, G., Springel, V., White, S. D. M., Lanzoni, B., Stoehr, F., Tormen, G., & Yoshida, N. 2004, *MNRAS*, 348, 333
- Diemand, J., Kuhlen, M., & Madau, P. 2007, *ArXiv Astrophysics e-prints*
- D’Onghia, E., Sommer-Larsen, J., Romeo, A. D., Burkert, A., Pedersen, K., Portinari, L., & Rasmussen, J. 2005, *ApJ*, 630, L109
- Elíasdóttir, Á., Limousin, M., Richard, J., Hjorth, J., Kneib, J.-P., Natarajan, P., Pedersen, K., Jullo, E., & Paraficz, D. 2007, *ArXiv e-prints*, 710
- Fischer, P., McKay, T. A., Sheldon, E., & The SDSS Collaboration. 2000, *AJ*, 120, 1198
- Geiger, B. & Schneider, P. 1999, *MNRAS*, 302, 118
- Ghigna, S., Moore, B., Governato, F., Lake, G., Quinn, T., & Stadel, J. 1998, *MNRAS*, 300, 146
- Gustafsson, M., Fairbairn, M., & Sommer-Larsen, J. 2006, *Phys. Rev. D*, 74, 123522
- Halkola, A., Seitz, S., & Pannella, M. 2007, *ApJ*, 656, 739
- Hoekstra, H., Franx, M., Kuijken, K., Carlberg, R. G., & Yee, H. K. C. 2003, *MNRAS*, 340, 609
- Hoekstra, H., Yee, H. K. C., & Gladders, M. D. 2004, *ApJ*, 606, 67
- Jørgensen, I., Chiboucas, K., Flint, K., Bergmann, M., Barr, J., & Davies, R. 2006, *ApJ*, 639, L9
- . 2007, *ApJ*, 654, L179
- Jørgensen, I., Franx, M., & Kjaergaard, P. 1996, *MNRAS*, 280, 167
- Jullo, E., Kneib, J.-P., Limousin, M., Elíasdóttir, A., Marshall, P., & Verdugo, T. 2007, *ArXiv e-prints*, 706
- Kneib, J.-P., Ellis, R. S., Smail, I., Couch, W. J., & Sharples, R. M. 1996, *ApJ*, 471, 643
- Lanzoni, B., Guiderdoni, B., Mamon, G. A., Devriendt, J., & Hatton, S. 2005, *MNRAS*, 361, 369
- Limousin, M., Kneib, J. P., Bardeau, S., Natarajan, P., Czoske, O., Smail, I., Ebeling, H., & Smith, G. P. 2007a, *A&A*, 461, 881
- Limousin, M., Kneib, J.-P., & Natarajan, P. 2005, *MNRAS*, 356, 309
- . 2006, *ArXiv Astrophysics e-prints*
- Limousin, M., Richard, J., Jullo, E., Kneib, J. P., Fort, B., Soucail, G., Elíasdóttir, A., Natarajan, P., Ellis, R. S., Smail, I., Czoske, O., Smith, G. P., Hudelot, P., Bardeau, S., Ebeling, H., Egami, E., & Knudsen, K. K. 2007b, *ApJ*, 668, 643
- Malumuth, E. M. & Richstone, D. O. 1984, *ApJ*, 276, 413
- Mamon, G. A. 2000, in *ASP Conf. Ser. 197: Dynamics of Galaxies: from the Early Universe to the Present*, ed. F. Combes, G. A. Mamon, & V. Charmandaris, 377–+
- McKay, T. A., Sheldon, E. S., Racusin, & et al. 2001, *ArXiv Astrophysics e-prints*
- Merritt, D. 1983, *ApJ*, 264, 24
- . 1984, *ApJ*, 276, 26
- Morales, M. F. 2006, *ApJ*, 650, L21
- Natarajan, P., De Lucia, G., & Springel, V. 2007, *MNRAS*, 376, 180
- Natarajan, P., Kneib, J.-P., & Smail, I. 2002a, *ApJ*, 580, L11
- Natarajan, P., Kneib, J.-P., Smail, I., & Ellis, R. S. 1998, *ApJ*, 499, 600
- Natarajan, P., Loeb, A., Kneib, J.-P., & Smail, I. 2002b, *ApJ*, 580, L17

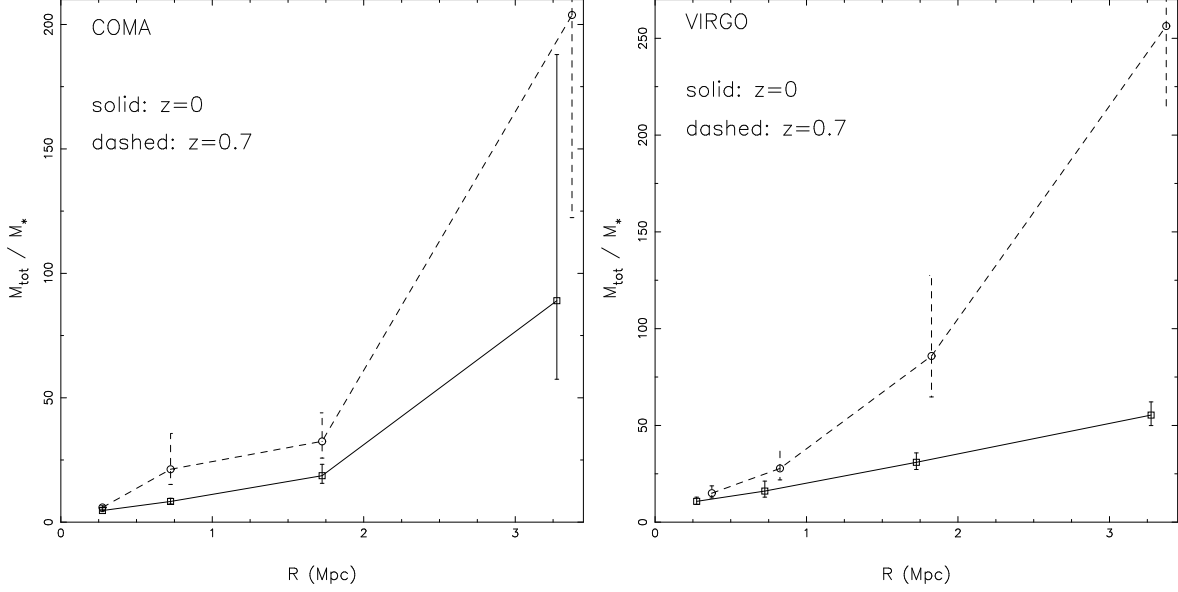


FIG. 4.— Median ratio of the total mass to the stellar mass of galaxies as a function of projected cluster-centric distance  $R$  at  $z=0$  and  $z=0.7$ . Left: COMA; right: VIRGO.

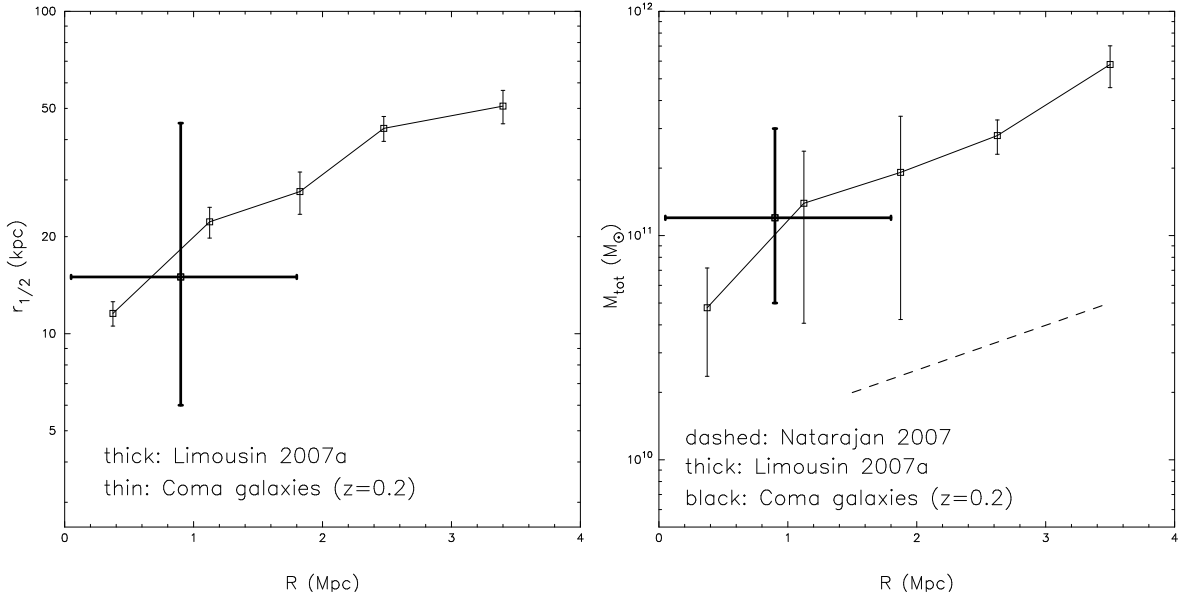


FIG. 5.— Comparison of Limousin et al.(2007a) and Natarajan et al.(2007) galaxy-galaxy lensing results with simulated COMA galaxies. Left panel:  $r_{1/2}$  versus cluster-centric radius; Right panel: total mass versus cluster-centric radius. To enable direct comparison with the lensing data, the same magnitude cut-off has been adopted in the simulations. The data point with error bars shown is derived from galaxy-galaxy lensing results averaged over the subhalo population ranging in cluster-centric radius from 0 to 1.8 Mpc for a sample of massive lensing clusters. The slope indicated with a dashed line shows the trend derived for Cl0024+16 from galaxy-galaxy lensing techniques as well by Natarajan et al. (2007) using space-based data. This trend is derived from mosaiced HST WFPC-2 data for Cl0024+16 out to 5 Mpc from the center. The slope corresponds to the change in subhalo mass with cluster-centric radius for a typical subhalo that hosts an early-type  $L^*$  galaxy. Note that the normalization cannot be compared directly due to the fact that the central density of Cl0024+16 is significantly larger than that of the simulated COMA studied here.

- Navarro, J. F., Frenk, C. S., & White, S. D. M. 1997, *ApJ*, 490, 493
- Prada, F., Vitvitska, M., Klypin, A., Holtzman, J. A., Schlegel, D. J., Grebel, E. K., Rix, H.-W., Brinkmann, J., McKay, T. A., & Csabai, I. 2003, *ApJ*, 598, 260
- Romeo, A. D., Portinari, L., & Sommer-Larsen, J. 2005, *MNRAS*, 361, 983
- Romeo, A. D., Sommer-Larsen, J., Portinari, L., & Antonuccio-Delogu, V. 2006, *MNRAS*, 371, 548
- Sommer-Larsen, J., Romeo, A. D., & Portinari, L. 2005, *MNRAS*, 357, 478
- Springel, V., Frenk, C. S., & White, S. D. M. 2006, *Nature*, 440, 1137
- Tyson, J. A., Kochanski, G. P., & dell'Antonio, I. P. 1998, *ApJ*, 498, L107+